Origin of Hund's multiplicity rule in quasi-two-dimensional two-electron quantum dots

Tokuei Sako[*]

Laboratory of Physics, College of Science and Technology, Nihon University, 7-24-1 Narashinodai, Funabashi, 274-8501 Chiba, Japan

Josef Paldus[†]

Department of Applied Mathematics, University of Waterloo, Waterloo, Ontario N2L 3G1, Canada

Geerd H. F. Diercksen[‡]

Max-Planck-Institut für Astrophysik, Karl-Schwarzschild-Strasse 1, D-85741 Garching, Germany

The origin of Hund's multiplicity rules has been studied for a system of two electrons confined by a quasi-two-dimensional harmonic-oscillator potential by relying on a full configuration interaction wave function and Cartesian anisotropic Gaussian basis sets. In terms of appropriate normal-mode coordinates the wave function factors into a product of the *center-of-mass* and the *internal* components. The $^1\Pi_u$ singlet state and the $^3\Pi_u$ triplet state represent the energetically lowest pair of states to which Hund's multiplicity rule applies. They are shown to involve excitations into different degrees of freedom, namely, into the center-of-mass angular mode and the internal angular mode for the singlet and triplet states, respectively. The presence of an angular nodal line in the internal space allows then the triplet state to avoid the singularity in the electron-electron interaction potential, leading to the energy lowering of the triplet state relative to its counterpart singlet state.

I. INTRODUCTION

Finite many-body quantum systems consisting of a small number of electrons bound in a fabricated nano-scale potential are referred to as quantum dots [1,2] or artificial atoms [3]. In recent years intense attention has been paid to these nano-sized objects as a source of new properties of matter. As in natural atoms, the electronic configurations of artificial atoms have been shown to follow Hund's multiplicity rule [4–6]. The Hund multiplicity rule is the first rule of Hund empirical rules [7] (see also Refs. [8–12]; for a historical outline see Refs. [13] and [14]). This first rule operates rigorously while the empirical nature of the other two rules was emphasized by Sommerfeld [15]. Note that the first rule also operates in the case of molecular species [16].

Hund's multiplicity rule states that among different spin states belonging to the same orbital configuration the highest total spin state has the lowest energy. The traditional interpretation of the origin of Hund's multiplicity rule was given by Slater in his 1929 article [17] in which he suggested that higher spin states weaken the electron-electron interaction potential (see also Refs. [10] and [11]). Later, Davidson [18,19] (see also Refs. [20–25]; for a review see Ref. [26]) actually evaluated the expectation values of the one-electron and two-electron operators at the Hartree-Fock level of approximation for the singlet-triplet pairs of a series of singly excited states of He, $(nl)^1 L$ and $(nl)^3 L$ ($n = 2, 3, \ldots$; $l = s, p, d, \ldots$; $L = S, P, D, \ldots$). On the basis of these

results he concluded, contrary to Slater's interpretation, that the triplet state, having the higher spin multiplicity, involves a larger energy increase due to the electron-electron repulsion potential than does the corresponding singlet state. This implies that the reason for a lower energy of the triplet state relative to the corresponding singlet state is not due to a decrease in the electron-electron interaction potential, but can be ascribed to a more compact electron density distribution of the triplet state, which then results in a much larger energy decrease due to the nuclear attraction potential that compensates the energy increase in the electron-electron repulsion potential [20–23,27].

In order to understand the origin of Hund's multiplicity rule for artificial atoms, in which the role of the electron repulsion potential varies strongly with the confinement strength [28–34], a full configuration interaction (CI) calculation has been carried out for a system of quasi-two-dimensional isotropic harmonic-oscillator quantum dots [35–38]. The second and the third Hund rules invoke spherical symmetry and, thus, do not directly pertain to the two-dimensional system studied in this article. Yet, it may be worthwhile to look for their analog in the presence of the cylindrical symmetry. A two-electron system has been chosen for this purpose, since a separation of the spin and the *center-of-mass* degrees of freedom permits insightful visualization of the internal part of the wave function, which in turn enables an unambiguous manifestation of the origin of Hund's multiplicity rule. Finally, we note that very recently the Hund rule was investigated for the three-dimensional, spherically symmetrical quantum dots confined by a rectangular potential [39].

———————

[*]sako@phys.ge.cst.nihon-u.ac.jp;   URL:http://www.phys.ge.cst.nihon-u.ac.jp/~sako/

[†]paldus@scienide2.uwaterloo.ca; URL:http://www.math.uwaterloo.ca/~paldus

[‡]ghd@mpa-garching.mpg.de; URL:http://www.mpa-garching.mpg.de/mol_physics/index.shtml

II. COMPUTATIONAL DETAILS

The Hamiltonian operator used in the present study for a model of quasi-two-dimensional two-electron quantum dots is

given by

$$\mathcal{H} = \sum_{i=1}^{2}\left[-\frac{1}{2}\nabla_i^2\right] + \sum_{i=1}^{2} w_{\text{q2D}}(\mathbf{r}_i) + \frac{1}{|\mathbf{r}_1 - \mathbf{r}_2|}, \qquad (1)$$

where the one-electron confining potential w_{q2D} has the form

$$w_{\text{q2D}}(\boldsymbol{r}) = \tfrac{1}{2}\omega_{xy}^2(x^2 + y^2) + \tfrac{1}{2}\omega_z^2 z^2. \qquad (2)$$

The effective atomic units are used throughout the article in which the unit length and energy correspond to 9.79 nm and 11.9 meV, respectively, for GaAs semiconductor quantum dots [40,41]. For sufficiently large values of ω_z, satisfying the condition $\omega_z \gg \omega_{xy}$, electrons bound by the potential of Eq. (2) are strongly compressed along the z direction and have degrees of freedom only within the xy plane. Therefore, under the condition $\omega_z \gg \omega_{xy}$, Eq. (2) represents a confining potential for quasi-two-dimensional harmonic-oscillator quantum dots with an oblate-top, disk-like shape. In the present study ω_z has been chosen to be 100 times larger than ω_{xy}, that is, $\omega_z = 100\omega_{xy}$. Since the results do not change qualitatively with a specific choice of ω_z, whose value is fixed by the value of ω_{xy}, its magnitude is not necessarily indicated explicitly hereafter.

The Schrödinger equation for the Hamiltonian of Eq. (1) has been solved by employing closed-shell Hartree-Fock orbitals in the full CI method. As basis set for the expansion of the one-particle Hartree-Fock orbitals properly chosen Cartesian anisotropic Gaussian-type orbitals (C-aniGTO) of appropriate size have been employed [31,42–44]. The high reliability of C-aniGTO basis sets for the calculation of properties of electrons confined by an anisotropic potential has been amply demonstrated in previous studies and will not be repeated here [45–53]. A total of 66 functions, sharing the common exponents ($\omega_{xy}/2$, $\omega_{xy}/2$, $\omega_z/2$) and designated as [1s1p1d1f1g1h1i1j1k1l1m] using the standard quantum chemical notation, have been used as the basis set. Here, the symmetry labels s, p, ... do not imply spherical symmetry but specify the number of nodes in each anisotropic orbital. Functions having nodes along the z coordinate are neglected [32,54].

III. RESULTS AND DISCUSSION

A. Energy spectrum

In case of two-electron He-like atoms it is straightforward to interpret the part of the energy spectrum that is situated below the first ionization limit, since it involves only one-electron excitations from the singlet ground state $(1s)^2$ ^1S. However, in the case of quantum dots, multiple excitations play a fundamental role in the understanding of their complex energy spectra [31,32,54]. It is convenient to start the analysis of the energy spectrum with the case that is referred to as the *large regime*, characterized by a large value of the confinement strength ω_{xy}, since in this case the complexity of the corresponding spectra is considerably reduced. Indeed, in this limit the electron correlation effects may be neglected to a good degree of approximation [28,33,34].

The energy spectrum of two electrons confined by the potential of Eq. (2) relative to the ground state is displayed in Fig. 1 for $\omega_{xy} = 10$, which corresponds to the large regime of
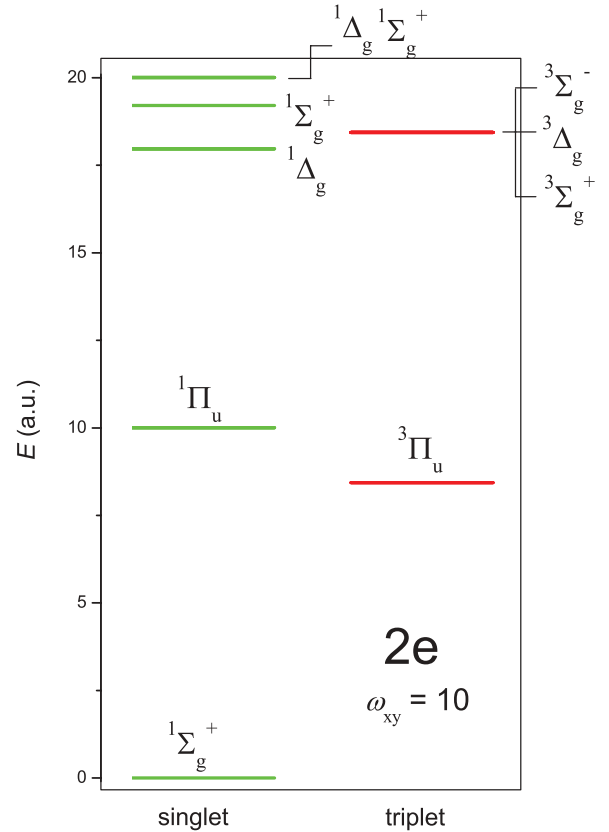

FIG. 1. (Color online) Energy spectrum of two electrons confined by a quasi-two-dimensional harmonic potential with $(\omega_{xy}, \omega_z) = (10, 1000)$ relative to the ground state energy. Energy levels of singlet and triplet states are rendered in green (light gray) and red (dark gray), respectively.

the confinement strength. The symbol ^{2S+1}A that is associated with each level represents the spin multiplicity $2S + 1$ and the spatial symmetry label A in the $D_{\infty,h}$ symmetry group. The fifth level in the singlet manifold and the second level in the triplet manifold are doubly and triply degenerate, respectively. These degeneracies are not accidental, but they are a consequence of the generalized Kohn theorem [55–60] which is revisited in Sec. III B.

The low-lying closed-shell Hartree-Fock orbitals are displayed in Fig. 2 in the order of increasing orbital energies. The orbitals are labeled by the symbol $[v_{xy}, v_z]a$ [32], with v_{xy}, v_z, and a representing the number of nodes within the xy plane, the number of nodes along the z axis, and the spatial symmetry label, respectively. Two types of nodes are observed in the xy plane: *angular nodes* originating from the angular momentum with respect to the z axis and circular *radial nodes* cutting the orbital circularly about the z axis, as displayed in Figs. 2(b), 2(c), and 2(d), respectively. The number of angular and radial nodes are designated by $|l_z|$ and n_r, respectively. They contribute to v_{xy} by $2n_r + |l_z|$. The reason for the twice-as-large contribution of n_r toward v_{xy} than that of $|l_z|$ has been amply discussed elsewhere [54]. The number of nodes v_z is zero for all orbitals covered by the present study, since an excitation into this mode requires an extremely large energy due to the strong confinement along the z axis.

(a) [0,0]σ_g

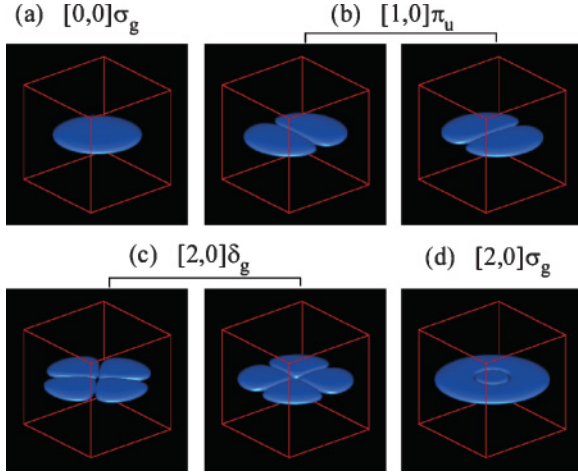## (b) [1,0]π_u

(c) [2,0]δ_g

(d) [2,0]σ_g

FIG. 2. (Color online) Closed-shell Hartree-Fock orbitals for two electrons confined by a quasi-two-dimensional harmonic potential with $(\omega_{xy}, \omega_z) = (10, 1000)$. The density at the surface is 0.05. The side length of the red cube is 2.0 a.u. The orbitals are labeled by $[v_{xy}, v_z]a$, where v_{xy}, v_z, and a represent the number of nodes in the xy plane, the number of nodes along the z axis, and the spatial symmetry label, respectively.

For the low-lying states that are displayed in Fig. 1, the leading configurations and the square moduli of their coefficients in the CI wave functions are listed in Table I. The *polyad quantum number* v_p [54], which is defined by the total number of nodes of the leading configuration in the CI wave functions and is equal to the sum of v_{xy} for two orbitals in the leading configuration, is also given in this table. The energy spectrum displayed in Fig. 1 shows a harmonic band structure, in which the energy levels with

TABLE I. Leading configurations and square moduli of their coefficients in the CI wave functions for the low-lying states of two electrons confined by the quasi-two-dimensional harmonic potential with $(\omega_{xy}, \omega_z) = (10, 1000)$. The symbols v_p and E specify the polyad quantum number and the relative energy from the lowest state, respectively.

v_p	E (a.u.)	State	Configuration	Coef.
0	0.000	$^1\Sigma_g^+$	$([0, 0]\sigma_g)^2$	0.995
1	8.437	$^3\Pi_u$	$([0, 0]\sigma_g)([1, 0]\pi_u)$	0.998
1	10.002	$^1\Pi_u$	$([0, 0]\sigma_g)([1, 0]\pi_u)$	0.993
2	17.968	$^1\Delta_g$	$([0, 0]\sigma_g)([2, 0]\delta_g)$	0.499
			$([1, 0]\pi_u)^2$	0.498
2	18.437	$^3\Sigma_g^+$	$([0, 0]\sigma_g)([2, 0]\sigma_g)$	0.997
2	18.438	$^3\Delta_g$	$([0, 0]\sigma_g)([2, 0]\delta_g)$	0.997
2	18.438	$^3\Sigma_g^-$	$([1, 0]\pi_u)([1, 0]\pi_u)$	0.996
2	19.208	$^1\Sigma_g^+$	$([0, 0]\sigma_g)([2, 0]\sigma_g)$	0.498
			$([1, 0]\pi_u)^2$	0.498
2	20.003	$^1\Sigma_g^+$	$([0, 0]\sigma_g)([2, 0]\sigma_g)$	0.498
			$([1, 0]\pi_u)^2$	0.490
2	20.004	$^1\Delta_g$	$([0, 0]\sigma_g)([2, 0]\delta_g)$	0.495
			$([1, 0]\pi_u)^2$	0.496

the same value of v_p are close together, while those having a different value of v_p are separated by multiples of ω_{xy}. This is a characteristic feature of the energy spectra of harmonic-oscillator quantum dots in the strong confinement regime [33,34].

The $^1\Sigma_g^+$ ground state has the leading configuration $([0, 0]\sigma_g)^2$, with the weight 0.995, showing that the ground state is dominated exclusively by the doubly occupied lowest orbital configuration. The first excited $^1\Pi$ singlet state and the lowest $^3\Pi$ triplet state have the same leading configuration $([0, 0]\sigma_g)([1, 0]\pi_u)$ with the weights 0.993 and 0.998, respectively. This implies that they form a singlet-triplet pair to which the Hund multiplicity rule applies.

On the other hand, in the case of the singlet manifold with $v_p = 2$, all three energy levels, namely, the two $^1\Sigma_g^+$ states and the one $^1\Delta_g$ state, involve two leading configurations having almost the same weights, indicating a strong configuration mixing. Furthermore, the two $^1\Sigma_g^+$ singlet states share the same set of two leading configurations, $([0, 0]\sigma_g)([2, 0]\sigma_g)$ and $([1, 0]\pi_u)^2$. Now, in this strong confinement regime of $\omega_{xy} = 10$, electron correlation should be negligibly small. Therefore, the large mixing of these two configurations in the strong confinement regime indicates an improper description of the states of quantum dots that is based on an independent electron model with Hartree-Fock orbitals. In order to properly describe the states in the $v_p = 2$ manifold, appropriate assignments of the *normal modes* of electrons are required [33,34,61]; these are introduced in the next section.

B. Normal-mode assignments

The normal coordinates for two electrons of the present model are obtained by transforming the independent electron coordinates (x_1, y_1, x_2, y_2) into

$$x_s = \frac{1}{\sqrt{2}}[x_1 + x_2],$$
$$y_s = \frac{1}{\sqrt{2}}[y_1 + y_2],$$
$$x_a = \frac{1}{\sqrt{2}}[x_1 - x_2],$$
$$y_a = \frac{1}{\sqrt{2}}[y_1 - y_2],$$

(3)

where z coordinates are neglected. The symmetric coordinates x_s and y_s represent the center-of-mass degrees of freedom, while the anti-symmetric coordinates x_a and y_a represent the internal degrees of freedom. Using these new coordinates and neglecting the dependence on the z coordinate, the Hamiltonian of Eq. (1) separates into the sum of two contributions, depending on either the coordinates (x_s, y_s) or (x_a, y_a), that is,

$$\mathcal{H}_{2D} = \mathcal{H}_{c.m.}(x_s, y_s) + \mathcal{H}_{int}(x_a, y_a),$$

(4)

where

$$\mathcal{H}_{c.m.} = -\frac{1}{2}\left[\frac{\partial^2}{\partial x_s^2} + \frac{\partial^2}{\partial y_s^2}\right] + \frac{1}{2}\omega_{xy}^2[x_s^2 + y_s^2],$$

(5)

and

$$\mathcal{H}_{\text{int}} = -\frac{1}{2}\left[\frac{\partial^2}{\partial x_a^2} + \frac{\partial^2}{\partial y_a^2}\right] + \frac{1}{2}\omega_{xy}^2[x_a^2 + y_a^2] + \frac{1}{\sqrt{2(x_a^2 + y_a^2)}}.$$
(6)

The Schödinger equation for the two-dimensional Hamiltonian $\mathcal{H}_{\text{2D}}$ and for its three-dimensional analog, that is, the Hamiltonian for two electrons confined in a spherical harmonic-oscillator potential, can be solved in a closed form for specific values of ω_{xy} [62,63].

The Hamiltonian $\mathcal{H}_{\text{c.m.}}$ is the Hamiltonian for a two-dimensional isotropic harmonic oscillator. Therefore, the eigenstates of $\mathcal{H}_{\text{c.m.}}$ are specified by the two quantum numbers n_s and l_s as $\Psi_{\text{c.m.}}^{n_s,l_s}$, where n_s and l_s represent the number of radial nodes and the angular momentum about the z axis, respectively, as for the Hartree-Fock orbitals in Fig. 2. The eigenenergy $E_{\text{c.m.}}$ is represented in terms of these quantum numbers as $E_{\text{c.m.}} = \omega_{xy}[2n_s + l_s + 2]$. The Hamiltonian $\mathcal{H}_{\text{int}}$ is then a sum of another two-dimensional isotropic harmonic-oscillator Hamiltonian and of a singular potential located at the center of the harmonic-oscillator potential. The latter originates from the electron repulsion potential. Since the potential energy function of $\mathcal{H}_{\text{int}}$ has an axial symmetry about the origin, the eigenstates of this Hamiltonian can also be labeled by a radial quantum number n_a and the angular momentum quantum number l_a as $\Psi_{\text{int}}^{n_a,l_a}$. Therefore, the eigenstates of the total Hamiltonian are labeled by the set of four normal-mode quantum numbers (n_s, l_s, n_a, l_a).

The Pauli principle imposes a restriction on the symmetry of $\Psi_{\text{int}}^{n_a,l_a}$ as follows. Exchanging the spatial coordinates of the electron 1 and 2 changes the sign of the antisymmetric coordinates as $(x_a, y_a) \rightarrow (-x_a, -y_a)$, while it does not affect the symmetric coordinates (x_s, y_s). Therefore, the eigenfunction for the center-of-mass degrees of freedom $\Psi_{\text{c.m.}}^{n_s,l_s}(x_s, y_s)$ is not affected by the Pauli principle and only the internal eigenfunction $\Psi_{\text{int}}^{n_a,l_a}$ is affected by it. Since the spin part of the wave function is separated from the spatial part for two-electron systems, $\Psi_{\text{int}}^{n_a,l_a}$ changes its sign with the exchange of the electron coordinates for triplet states but not for singlet states.

The relation between this symmetry restriction and the quantum numbers (n_a, l_a) can be established by transforming the Cartesian coordinates (x_a, y_a) into the polar coordinates (r_a, θ_a), where $x_a = r_a \cos\theta_a$ and $y_a = r_a \sin\theta_a$. By using these polar coordinates the internal eigenfunction becomes

$$\Psi_{\text{int}}^{n_a,l_a} = \psi_{n_a}(r_a)\exp(il_a\theta_a),$$
(7)

where the polar angle θ_a is the conjugate variable to the angular momentum l_a. Inverting the Cartesian coordinates, $(x_a, y_a) \rightarrow (-x_a, -y_a)$, corresponds to the transformation $(r_a, \theta_a) \rightarrow (r_a, \theta_a + \pi)$ in terms of the polar coordinates. Therefore, as implied by Eq. (7), the internal eigenfunction is transformed with respect to the interchange of electron coordinates as $\Psi_{\text{int}}^{n_a,l_a} \rightarrow (-1)^{l_a}\Psi_{\text{int}}^{n_a,l_a}$. As a result the singlet and triplet states must be labeled by even and odd values of l_a, respectively.

The eigenenergy $E_{\text{int}}^{n_a,l_a}$ of the internal Hamiltonian relative to the energy of the lowest state and the plot of the square

density of the internal eigenfunction $\Psi_{\text{int}}^{n_a,l_a}$ are displayed in Fig. 3 for the same energy region as in Fig. 1. The ω_{xy}-scaled dimensionless internal coordinates $(x_a\sqrt{\omega_{xy}}, y_a\sqrt{\omega_{xy}})$ have been used in the density plots for convenience in the later discussion concerning the dependence of the results on the confinement strength. For comparison, the spectrum of the total energy has also been plotted on the left-hand side of the figure.

As seen from Fig. 3 for some levels in the total energy spectrum a corresponding level in the internal energy spectrum located at nearly the same height can be found while for some levels this is not the case. For example, the $^1\Sigma_g^+$ ground state and the $^3\Pi_u$ lowest triplet state have such a corresponding level, while the first excited $^1\Pi_u$ singlet state has no counterpart in the internal energy spectrum. Since the total energy is the sum of $E_{\text{c.m.}}$ and E_{int}, and since $E_{\text{c.m.}}$ is the eigenenergy of a harmonic oscillator, those levels having a corresponding level in the internal energy spectrum are associated with the states that have no excitation into the center-of-mass degrees of freedom, namely, those labeled by $(0, 0, n_a, l_a)$. The remaining states that have no counterpart in the internal energy spectrum are generated from the internal states by exciting the center-of-mass modes, and their energy is given by the sum of the internal energy and of a multiple of ω_{xy}.

Assignments that are based on the four normal-mode quantum numbers (n_s, l_s, n_a, l_a) for the low-lying states, displayed in Figs. 1 and 3, are given in Table II. The $^1\Sigma_g^+$ ground state involves neither an excitation into the center-of-mass mode nor an excitation into the internal mode. The lowest $^3\Pi_u$ triplet state involves an excitation of one quantum into the angular mode of the internal degrees of freedom, as can be seen from the density plot in Fig. 3. Since this state has no excitation into the center-of-mass mode, the total angular momentum quantum number of this state, calculated as $|l_s + l_a|$, equals 1, which agrees with the symmetry label of this Π_u state. On the other hand, the first excited $^1\Pi_u$ singlet state, which is a singlet counterpart to the $^3\Pi_u$ triplet state according to Hund's multiplicity rule, has no excitation into

TABLE II. Assignments based on the normal-mode quantum numbers (n_s, l_s, n_a, l_a) for the low-lying states displayed in Table I. $|l_s + l_a|$ specifies the total angular momentum of the state. See the caption of Table I for other remarks.

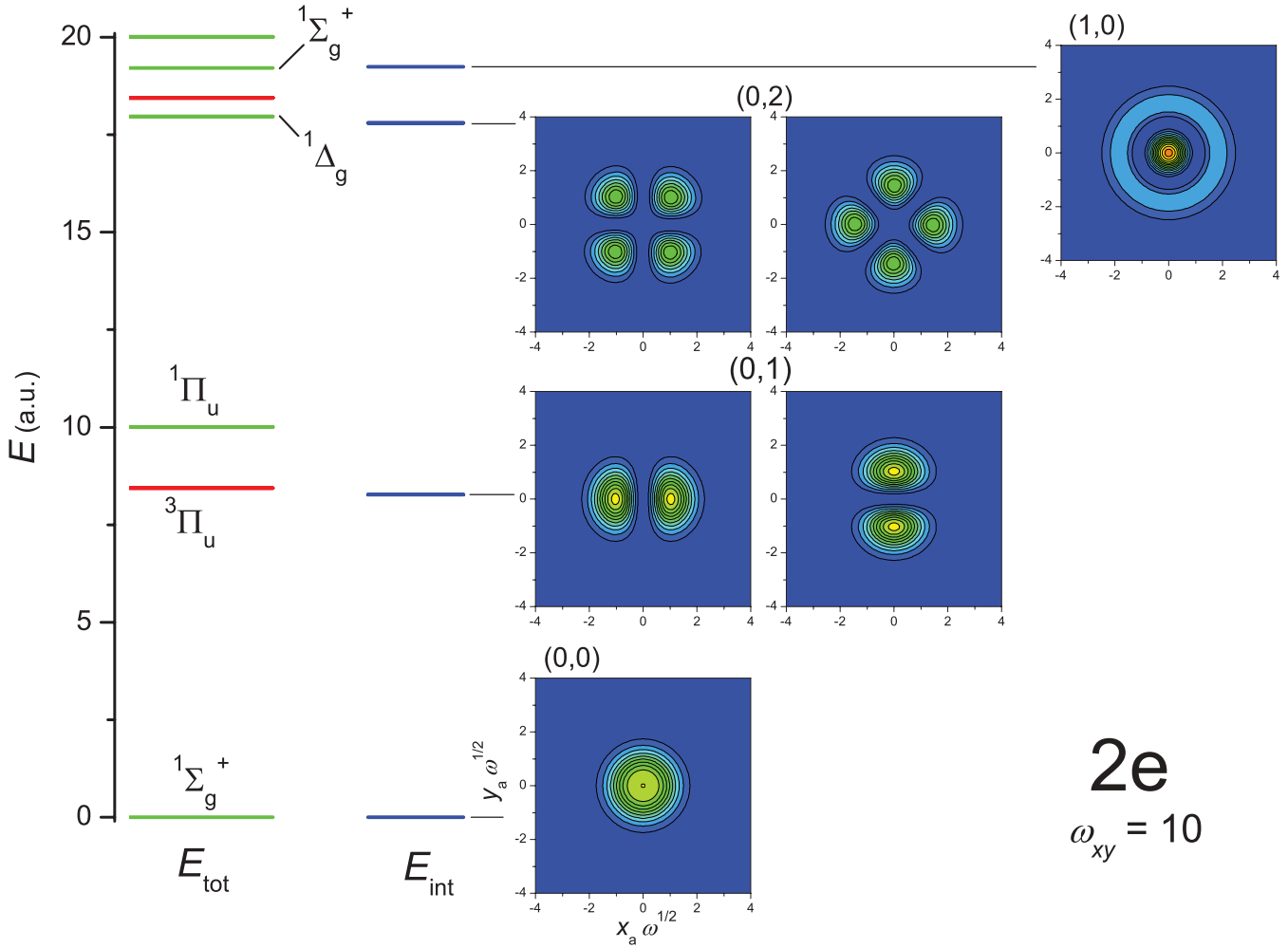| v_p	E (a.u.)	State	n_s	l_s	n_a	l_a	$|l_s + l_a|$
0	0.000	$^1\Sigma_g^+$	0	0	0	0	0
1	8.437	$^3\Pi_u$	0	0	0	± 1	1
1	10.002	$^1\Pi_u$	0	± 1	0	0	1
2	17.968	$^1\Delta_g$	0	0	0	± 2	2
2	18.437	$^3\Sigma_g^+$	0	$+1$	0	-1	0
			0	-1	0	$+1$	0
2	18.438	$^3\Delta_g$	0	$+1$	0	$+1$	2
			0	-1	0	-1	2
2	18.438	$^3\Sigma_g^-$	0	$+1$	0	-1	0
			0	-1	0	$+1$	0
2	19.208	$^1\Sigma_g^+$	0	0	1	0	0
2	20.003	$^1\Sigma_g^+$	1	0	0	0	0
2	20.004	$^1\Delta_g$	0	± 2	0	0	2

FIG. 3. (Color online) Eigenenergies and square density plot of the eigenfunctions for the internal Hamiltonian $\mathcal{H}_{\text{int}}$ with $\omega_{xy} = 10$. The eigenenergies E_{int} (blue short bar) are represented as relative energy with respect to the lowest state. The vertical and horizontal axes of the density plots are the scaled internal coordinates $x_a\sqrt{\omega_{xy}}$ and $y_a\sqrt{\omega_{xy}}$, respectively. The label $(n_a, |l_a|)$ given to the density plots represents the number of radial nodes n_a and the modulus of the angular momentum l_a, respectively. The spectrum of the total energy E_{tot} is plotted on the left-hand side for comparison (see also the caption to Fig. 1 for the remarks on the spectrum).

the internal degrees of freedom, but instead has an excitation of one quantum into the angular mode of the center-of-mass degree of freedom. Therefore, although this singlet-triplet pair of states has the same orbital configuration in terms of Hartree-Fock orbitals, there is a significant difference in terms of the normal-mode description since these singlet and triplet states involve an excitation into different degrees of freedom, that is, the center-of-mass for the singlet and the internal angular degree of freedom for the triplet. It is also noted that the $^1\Pi_u$ and $^3\Pi_u$ states are associated with the $|l_a|$ value equal to 0 and 1, respectively. This is a consequence of the Pauli principle requiring even and odd values of l_a for singlets and triplets, respectively.

Another observation concerning the first excited $^1\Pi$ singlet state that can be made on the basis of the values of Table II is the fact that the excitation energy of 10.002 a.u. relative to the ground state is very close to the value of ω_{xy}. This is again no accident but another consequence of the generalized Kohn theorem. Radiative transitions occur through a dipole operator such as $\sum_{i=1}^{2} \mathbf{r}_i$ in the length gauge. Since this operator is

proportional to the center-of-mass coordinates, it only affects the center-of-mass part of the wave functions $\Psi_{\text{c.m.}}^{n_s, l_s}$, resulting in an excitation energy equal to the harmonic-oscillator energy ω_{xy}. The tiny difference between the exact value of ω_{xy} and the calculated energy comes from the limited size of the basis set.

By adopting the normal-mode assignments given in Table II, the energy levels belonging to the $v_p = 2$ manifold, which appear to be rather complicated in an independent electron picture in terms of Hartree-Fock orbitals, can be rationalized as follows: First, the lowest energy $^1\Delta_g$ state in this manifold arises by the excitation of two quanta into the internal angular mode and no excitation into the other modes. In analogy to the $^1\Pi_u$-$^3\Pi_u$ pair, a counterpart triplet state should have the same value of v_p but possess one more quantum in the internal angular mode and one quantum less in the center-of-mass modes. Since, however, this $^1\Delta_g$ state has no excitation into the center-of-mass modes it cannot form a triplet state by transferring one quantum from the center-of-mass mode to the internal angular mode. Therefore, there is no counterpart triplet state to this singlet state as seen in the energy spectrum of

Fig. 1. Next, the three triplet states of this manifold, $^3\Sigma_g^+$, $^3\Delta_g$, and $^3\Sigma_g^-$, have practically the same energy and their excitation energies relative to the lowest $^3\Pi_u$ triplet state equal ω_{xy} within an accuracy of 1×10^{-3} a.u., implying that the excitation to these states from the $^3\Pi_u$ state is dipole-allowed. This observation can be confirmed by the normal-mode assignments in Table II. All these three states involve one quantum both in the internal angular mode and in the center-of-mass angular mode, that is, $|l_a| = |l_s| = 1$. Their differences lie in the mutual signs between l_a and l_s. In the case of the $^3\Delta_g$ state the two angular momenta l_a and l_s have the same sign. As a result, the total angular momentum $|l_s + l_a|$ of this state is 2, which agrees with the symmetry label of the $^3\Delta_g$ state. On the other hand, in the case of both $^3\Sigma_g$ states, $^3\Sigma_g^+$ and $^3\Sigma_g^-$, the two angular momenta l_a and l_s have mutually opposite signs, so that their total angular momentum vanishes. Since there are two sets of (l_s, l_a) quantum numbers yielding the zero angular momentum state, namely, $(1, -1)$ and $(-1, 1)$, there should result two $^3\Sigma_g$ states from these configurations. The sum and the difference of these states gives rise to the symmetric $^3\Sigma_g^+$ state and to the antisymmetric $^3\Sigma_g^-$ state, respectively.

A new phenomenon arises in the $^1\Sigma_g^+$ state at $E = 19.208$ a.u. in which case the internal radial mode is excited for the first time with one quantum. Since the number of radial nodes contributes to the polyad quantum number v_p by twice their number, the v_p value of this state is 2. Since this $^1\Sigma_g^+$ state has no excitation into the center-of-mass mode there is no triplet counterpart to it that would arise by transferring a quantum from the center-of-mass mode to the internal angular mode.

For the remaining two singlet states in the $v_p = 2$ manifold, $^1\Sigma_g^+$ and $^1\Delta_g$, with the relative energies $E = 20.003$ and 20.004, respectively, the excitation energy relative to the $^1\Pi_u$ state almost equals ω_{xy}, implying that they are the dipole-allowed states from the $^1\Pi_u$ state. From these $^1\Sigma_g^+$ and $^1\Delta_g$ states the counterpart triplet states, $^3\Sigma_g^+$ and $^3\Delta_g$, respectively, can be derived as follows. The $^1\Sigma_g^+$ has the normal-mode assignment of $(n_s, l_s, n_a, l_a) = (1, 0, 0, 0)$. Since this state has one quantum in the center-of-mass degree of freedom, triplet state can be derived by transferring one quantum into the internal angular mode. But since one quantum in the radial mode amounts to two quanta in the angular mode, transferring one quantum into the internal angular l_a mode leaves one quantum in the center-of-mass angular l_s mode. In order to preserve the original vanishing total angular momentum $|l_s + l_a|$, the possible combinations of (l_s, l_a) are $(1, -1)$ and $(-1, 1)$. Taking their symmetric linear combination gives rise to the triplet $^3\Sigma_g^+$ state. Similarly, in the case of the $^1\Delta_g$ state that possesses two quanta in the center-of-mass angular mode, the counterpart $^3\Delta_g$ state can be formed by transferring one quantum into the internal angular mode. In the next section the origin of Hund's multiplicity rule is clarified in terms of these normal-mode assignments.

C. Origin of Hund's multiplicity rule

As has been seen in the previous section there are two candidates for singlet-triplet pairs in the energy spectrum displayed in Fig. 1 that should obey Hund's multiplicity rule.
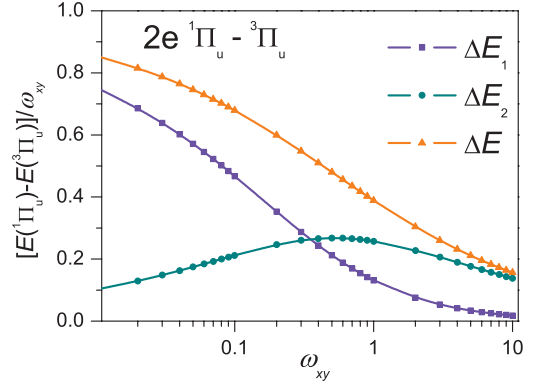

FIG. 4. (Color online) Energy differences between the lowest singlet-triplet pair of states, $^1\Pi_u$ and $^3\Pi_u$, for two electrons confined by a quasi-two-dimensional harmonic potential for different ω_{xy}. ΔE_1, ΔE_2, and ΔE represent the difference of the one-electron energy, two-electron energy, and the total energy, respectively, in units of ω_{xy}.

The first one is the $^1\Pi_u$-$^3\Pi_u$ pair in the $v_p = 1$ manifold, and the other candidate is the degenerate pair $^1\Delta_g$-$^3\Delta_g$ and $^1\Sigma_g^+$-$^3\Sigma_g^+$ in the $v_p = 2$ manifold. Since the latter pairs are simply replicas of the first pair, shifted toward the higher energy region by ω_{xy} as a consequence of the generalized Kohn theorem, the following analysis focuses on the first $^1\Pi_u$-$^3\Pi_u$ pair.

Three energy differences between the $^1\Pi_u$ and $^3\Pi_u$ states, namely, the one-electron energy ΔE_1, the two-electron energy ΔE_2, and the total energy ΔE, are plotted in Fig. 4 for different ω_{xy} values. The vertical energy axis in this figure is normalized by ω_{xy}, so that the results for different ω_{xy} values can be easily compared. The one-electron energy E_1 has been calculated by evaluating the expectation value of the sum of one-electron operators in the Hamiltonian (1) over the CI eigenfunctions, while the two-electron energy E_2 has been obtained by subtracting E_1 from the total energy E. Therefore, the three energy differences, ΔE_1, ΔE_2, and ΔE satisfy the relation

$$\Delta E = \Delta E_1 + \Delta E_2. \qquad (8)$$

As shown in Fig. 4, the total energy difference ΔE (orange triangles) increases significantly as ω_{xy} decreases from its initial value of 10. This implies that the energy splitting between the singlet and triplet levels is larger for smaller ω_{xy} than for the larger ones. For large values of ω_{xy}, such as $\omega_{xy} = 10$, the relative contribution of ΔE_1 and ΔE_2 to the total energy difference ΔE is almost exclusively ascribed to ΔE_2. This implies that in this large ω_{xy} regime the interpretation of the energy difference between different spin multiplets is closer to that of Slater rather than to that for the helium atom. A similar trend of the dominance of the two-electron contribution to the singlet-triplet energy difference was also reported for a system of two electrons confined by a spherically symmetric rectangular potential [39]. On the other hand, as ω_{xy} decreases, so does ΔE_2, while ΔE_1 increases. Consequently, the interpretation of the multiplicity rule becomes closer to that found for the helium case.

The square radial electron density distributions of the singlet-triplet pair of the $^1\Pi_u$ and $^3\Pi_u$ states are shown in Fig. 5
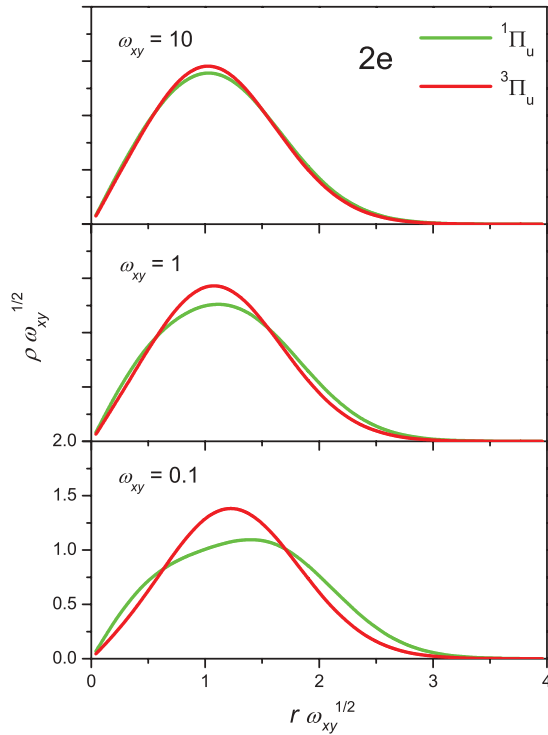
FIG. 5. (Color online) Square radial electron density distributions of the $^1\Pi_u$-$^3\Pi_u$ singlet-triplet pair of states for two electrons confined by a quasi-two-dimensional harmonic potential for $\omega_{xy} = 10$, 1, and 0.1. The horizontal axis represents the dimensionless, scaled radial coordinate $r\sqrt{\omega_{xy}}$. The green (light gray) and red (dark gray) curves represent the density distributions of the $^1\Pi_u$ singlet state and of the $^3\Pi_u$ triplet state, respectively.

for $\omega_{xy} = 10$, 1, and 0.1, as a function of the dimensionless scaled radial coordinate $r\sqrt{\omega_{xy}}$. For the sake of comparison, the square electron density distributions of the corresponding states of the helium atom, $(2p)\,^1P$ and $(2p)\,^3P$, are plotted in Fig. 6 (cf. also Fig. 2 of Ref. [39]). These electron density distributions of He were calculated using a full CI wave function of the He atom, obtained with the even-tempered
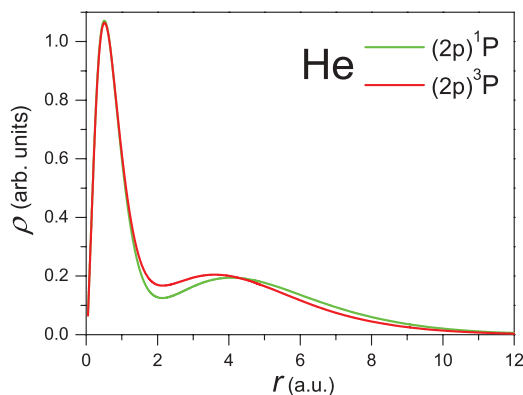

FIG. 6. (Color online) Square electron density distributions of the $(2p)\,^1P$-$(2p)\,^3P$ singlet-triplet pair of states of the helium atom as a function of the spherical radial coordinate r. The green (light gray) and red (dark gray) curves represent the density distribution of the $(2p)\,^1P$ singlet state and of the $(2p)\,^3P$ triplet state, respectively.

uncontracted Cartesian basis set $[10s7p5d]$ that was employed in our previous study [43].

The density distributions of He reveal that their inner part, having a sharp peak at around $r = 0.5$, is almost the same for the $(2p)\,^1P$ and $(2p)\,^3P$ states. Since this component of the density distribution originates primarily from $1s$ orbitals which are tightly bound to the nucleus, only marginal differences between the singlet and triplet states are found in this region. Thus, the only significant difference is found in the outer region, near the second broad peak in the density distribution. In the outer tail for $r > 5$ the density distribution for the singlet, represented by the green (light grey) curve in Fig. 6, is larger than that of the triplet state, represented by the red (dark grey) curve. The deficient density of the triplet state in this region reappears in an inner region around $r = 2.2$, where the triplet state has a larger density than the singlet state. These observations imply that the density distribution of the triplet state is on the average closer to the nucleus than that of the singlet state [20,21,23]. As shown by Davidson [18,19] and later by others, this compact density distribution of the triplet state results in a larger energy *increase* in the electron repulsion potential, yet a much larger energy *decrease* in the nuclear attraction potential than is the case for the corresponding singlet state. These two opposite contributions to the total energy result in the lowering of the triplet level relative to the singlet one, even though a simple reason for the compact density distribution of the triplet state is still lacking.

On the other hand, as is apparent from Fig. 5, the electron density distributions for the $^1\Pi_u$ and $^3\Pi_u$ states of the studied quantum dot are almost identical for $\omega_{xy} = 10$, except for a small difference in the height of their peaks. Since their electron density distributions are almost the same, their one-electron energies should also be nearly equal to each other. This agrees with the energy differences displayed in Fig. 4, where the one-electron energy difference ΔE_1 is very small while the difference in the two-electron energy ΔE_2 is primarily responsible for the singlet-triplet energy gap. A similar trend in the increase of the importance of the two-electron contribution relative to the nuclear attraction with increasing nuclear charge has been reported for highly charged atomic cations, in which the electron density distribution is highly contracted around the nucleus [24–26]. As the confinement strength decreases to $\omega_{xy} = 1.0$, the density distribution of the singlet state, represented by the green (light grey) curve, peaks at a slightly larger value of $r\sqrt{\omega_{xy}}$ and becomes slightly broader, while that of the triplet state, represented by the red (dark grey) curve, remains almost the same as in the $\omega_{xy} = 10$ a.u. case. When the confinement strength is further decreased to $\omega_{xy} = 0.1$, the density distribution of the singlet state become even broader with the peak position shifted strongly toward larger r values, while that of the triplet state preserves almost the same shape with a slightly shifted peak position toward the region of larger r values.

In order to rationalize these observations, based on the results shown in Figs. 4 and 5, namely, the change in the energy differences ΔE_1 and ΔE_2 and the evolution of the electron density distributions with ω_{xy}, and, more fundamentally, to understand the mechanism of why the triplet $^3\Pi_u$ state always has a lower energy than the singlet $^1\Pi_u$ state in the whole range of ω_{xy}, the *potential energy function* defined by a sum
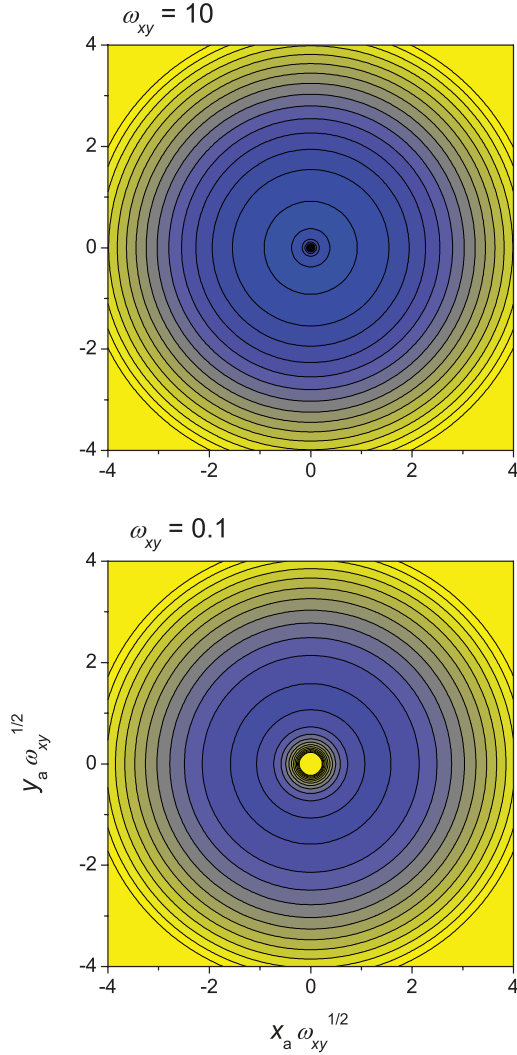
FIG. 7. (Color online) Contour plot of the potential energy function defined by the sum of the one- and two-electron potentials within the internal space for $\omega_{xy} = 10$ (upper figure) and 0.1 (lower figure). The horizontal and vertical axes represent ω_{xy}-scaled internal coordinates, $x_a\sqrt{\omega_{xy}}$ and $y_a\sqrt{\omega_{xy}}$, respectively. The maximum energy contour displayed in the plot is $10\omega_{xy}$.

of one-electron and two-electron potentials within the internal space, namely, the potential part of the internal Hamiltonian $\mathcal{H}_{int}$ of Eq. (6), has been plotted in Fig. 7 for both the large and small confinement regimes as represented by $\omega_{xy} = 10$ and 0.1, respectively. In this figure the potential energy function is represented in the ω_{xy}-scaled dimensionless internal coordinates, namely, $x_a\sqrt{\omega_{xy}}$ and $y_a\sqrt{\omega_{xy}}$. The maximum energy of contours plotted in this figure amounts to $10\omega_{xy}$. When the electron-electron interaction is neglected in this representation the potential energy functions for $\omega_{xy} = 10$ and 0.1 become essentially identical. Therefore, this figure clearly reveals the effect of the electron-electron interaction.

As seen in Fig. 7 the yellow (light grey) spot in the center of the potential energy function, representing a sharp increase of the energy due to the electron-electron repulsion potential, becomes larger as ω_{xy} decreases from 10 to 0.1. This implies that the effect of the electron-electron interaction becomes

stronger as the confinement strength ω_{xy} becomes smaller. This can be easily understood by rewriting the potential energy function in terms of the scaled internal coordinates as follows:

$$V_{int}/\omega_{xy} = \frac{1}{2}\left(\tilde{x}_a^2 + \tilde{y}_a^2\right) + \frac{1}{\sqrt{\omega_{xy}}}\frac{1}{\sqrt{2\left(\tilde{x}_a^2 + \tilde{y}_a^2\right)}}, \quad (9)$$

where $\tilde{x}_a$ and $\tilde{y}_a$ represent the scaled coordinates $x_a\sqrt{\omega_{xy}}$ and $y_a\sqrt{\omega_{xy}}$, respectively. The second term on the right-hand side of Eq. (9), representing the electron-electron repulsion potential, is scaled with respect to ω_{xy} by $\frac{1}{\sqrt{\omega_{xy}}}$. Therefore, this term becomes increasingly stronger as ω_{xy} becomes smaller.

By relying on this potential energy function the origin of Hund's multiplicity rule in the quasi-two-dimensional quantum dots can be rationalized as follows: The total wave function, i.e., both of the center-of-mass component $\Psi_{c.m.}$ and the internal part Ψ_{int} of the $^1\Pi_u$ singlet and $^3\Pi_u$ triplet states is shown in Fig. 8 for $\omega_{xy} = 10$ and 0.1. As is apparent from Table II, the $^1\Pi_u$ singlet and $^3\Pi_u$ triplet states are characterized by the normal-mode assignments $(0, \pm1, 0, 0)$ and $(0, 0, 0, \pm1)$, respectively, implying that the singlet state involves an excitation of one quantum into the center-of-mass angular mode, while the triplet state involves an excitation into the internal angular mode. Should there be no electron-electron interaction, the internal wave function Ψ_{int} would represent the eigenfunction of the two-dimensional isotropic harmonic oscillator with frequency ω_{xy}; that is, it would be identical to the corresponding $\Psi_{c.m.}$ wave function having the same set of quantum numbers. Therefore, in this case these two total wave functions of singlet and triplet states in Fig. 8 should have the same energy, since they involve the same total number of nodes. Quite a different situation arises, however, in the presence of the electron repulsion potential that appears only in the internal space and is characterized by a sharp pole-like singularity in the potential energy, as displayed in Fig. 7. In the case of the $^3\Pi_u$ triplet state, the internal wave function Ψ_{int} is only insignificantly influenced by this pole, since its density in the neighborhood of this singularity is negligible, that is, at the origin of the internal space, owing to the nodal line passing through the origin, as displayed in Fig. 8. On the other hand, in the case of the $^1\Pi_u$ singlet state, the internal wave function is significantly influenced by the pole, since it has a finite density at the singularity region. Thus, the $^3\Pi_u$ triplet state has an energy lower than that of the corresponding $^1\Pi_u$ singlet state.

As the confinement strength ω_{xy} becomes smaller, the electron-electron interaction potential becomes stronger relative to the harmonic-oscillator confining potential as implied by Eq. (9). Indeed, the pole at the center of the potential energy function, as displayed in Fig. 7, significantly increases in size. Consequently, it should exhibit a larger influence on the internal wave functions for $\omega_{xy} = 0.1$. In the case of the $^3\Pi_u$ triplet state the internal wave function Ψ_{int} can still avoid the effect of the singularity at the pole thanks to the presence of its nodal line. The width of the nodal region is, however, larger in this case than for $\omega_{xy} = 10$, indicating that the electrons avoid the central region where the potential energy is very high due to the electron repulsion potential. In the case of the $^1\Pi_u$ singlet
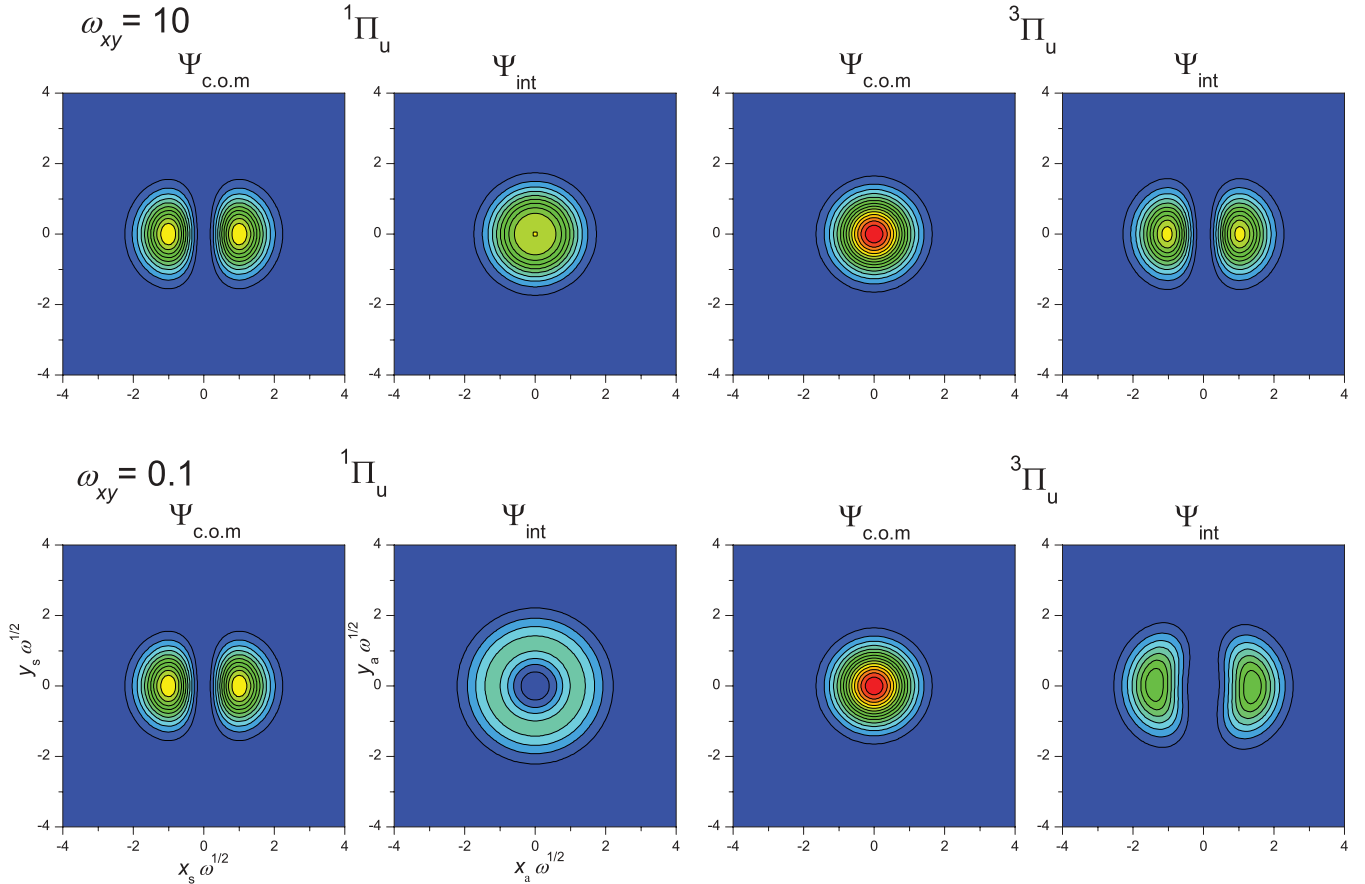
FIG. 8. (Color online) Square-density plot of the center-of-mass and internal parts of the wave function of the $^1\Pi_u$ singlet state (left) and of the $^3\Pi_u$ triplet state (right) for $\omega_{xy} = 10$ (upper) and 0.1 (lower). The horizontal and vertical axes represent the ω_{xy}-scaled dimensionless coordinates, $(x_s\sqrt{\omega_{xy}},\ y_s\sqrt{\omega_{xy}})$ for the center-of-mass part $\Psi_{\text{c.m.}}$ and $(x_a\sqrt{\omega_{xy}},\ y_a\sqrt{\omega_{xy}})$ for the internal part Ψ_{int}, respectively. Only the x component of the doubly degenerate Π state is displayed in this figure for both $^1\Pi_u$ and $^3\Pi_u$ states.

state the internal wave function has a "hole" at the center for $\omega_{xy} = 0.1$, as shown in the second row of Fig. 8. Of course, the internal wave function of this state should not have a node since this is the lowest eigenstate of the internal Hamiltonian $\mathcal{H}_{\text{int}}$. In fact, the hole in this internal wave function is not a real node, but rather a low-density area where the electron density practically vanishes. This hole region is created by the large singular region in the neighborhood of the potential pole that strongly expels the electrons from this region. The electron density which is suppressed in this central region by the potential pole expands the internal wave function as displayed in Fig. 8, resulting in the deformation of the electron density distribution of the singlet state as has been observed in Fig. 5. The large difference in the electron density distributions between the singlet and triplet states for small ω_{xy} results in a significant difference in their one-electron energies. This explains the reason why for smaller ω_{xy} the partition of the total energy difference into the one- and two-electron contributions becomes closer to that of the helium case rather than to that of Slater's.

The mechanism for the lowering of the triplet state energy relative to the corresponding singlet state in quasi-two-dimensional, two-electron quantum dots can be summarized as follows: The singlet and triplet states, which comprise the Hund multiplicity pairs, are characterized by the normal-mode quantum numbers (n_s, l_s, n_a, l_a) for the former state and by either $(n_s, l_s - 1, n_a, l_a + 1)$ or $(n_s - 1, l_s + 1, n_a, l_a + 1)$ for the latter states. The larger quantum number in the internal angular mode for triplets enables these to avoid more efficiently the singularity in the electron repulsion potential than in the case for the corresponding singlet states, leading to a lower energy of triplets relative to singlets.

IV. SUMMARY

The present study considers the low-lying states of two electrons confined by a quasi-two-dimensional harmonic-oscillator potential that lies below the $v_p = 2$ polyad manifold, as described by the full CI method employing Cartesian anisotropic Gaussian basis sets. The primary objective is to elucidate the origin and nature of the Hund multiplicity rule for two-electron quantum dots and its relationship to the mechanism operating in atomic or molecular systems. Analysis of the pertinent CI wave functions reveals that above the $v_p = 1$ manifold they involve more than one leading Hartree-Fock reference even in the large confinement regime where the effect of electron correlation is negligibly small. This indicates the shortcomings of a description of the quantum

dot states that is based on an independent electron model using Hartree-Fock orbitals. The introduction of normal-mode coordinates enables a factorization of the wave functions into a product of two independent components, namely, the center-of-mass $\Psi_{c.m.}$ and the internal Ψ_{int} wave functions. Each of these component wave functions can be labeled by a set of two quantum numbers: the radial quantum number n and the angular momentum quantum number l, designated as (n_s, l_s) and (n_a, l_a) for $\Psi_{c.m.}$ and Ψ_{int}, respectively. A unified normal-mode assignment adopting these four quantum numbers, (n_s, l_s, n_a, l_a), has been successfully made for all the eigenstates covered in the present study for the large confinement regime of $\omega_{xy} = 10$.

The $^1\Pi_u$ singlet and $^3\Pi_u$ triplet states in the $v_p = 1$ manifold have been chosen as a typical example to study Hund's multiplicity rule in quasi-two-dimensional quantum dots. The energy separation characterizing this lowest singlet-triplet pair significantly increases in terms of the normalized energy unit as the confinement strength ω_{xy} decreases. This energy separation is shown to be primarily due to the difference in the two-electron energy for large ω_{xy}, implying that it is closer to Slater's interpretation than to that found for the atomic helium. As ω_{xy} decreases, the contribution of the one-electron energy becomes larger while that of the two-electron energy becomes relatively smaller, implying that the energy partitioning into the one- and two-electron contributions approaches that characterizing the helium case. The radial electron density distributions have been also examined for different values of ω_{xy}. For $\omega_{xy} = 10$ these distributions are almost identical in the singlet and triplet states, while they increasingly differ as ω_{xy} becomes smaller: the singlet state electron density distribution becomes broader and its shape becomes gradually deformed as ω_{xy} decreases while the distribution of the triplet state density remains almost the same except for a small shift of the peak position toward the region of larger r values.

In order to rationalize the observed evolution of the energy differences and the electron density distributions of the singlet-triplet pair for different values of ω_{xy}, the nodal patterns of the center-of-mass and the internal wave functions have been examined. It appears that the singlet-triplet pair of states having the same orbital configuration in terms of Hartree-Fock orbitals involves an excitation into different degrees of freedom, namely, the center-of-mass angular mode for the singlet and the internal angular mode for the triplet. Thanks to a nonzero angular momentum in the internal degree of freedom, the $^3\Pi_u$ triplet state avoids the singularity of the electron repulsion potential, since the angular nodal line

passes through the origin. On the other hand, in the case of the $^1\Pi_u$ singlet state, the internal wave function has no node and thus a finite density in the region of singularity. Consequently, the triplet state has always an energy lower than that of the counterpart singlet state. This situation is the same for smaller ω_{xy} as well, yet the electron repulsion potential has more profound influence on the internal wave function. As a result, the electron density distribution of the singlet state is more strongly deformed than that of the triplet state. The large difference in the electron density distributions between the singlet and triplet states for small ω_{xy} results in a significant difference in their one-electron energies, which in turn makes the one-electron contribution to the singlet-triplet energy splitting dominate the two-electron contribution.

In closing, let us remark that the present study provides an unambiguous manifestation of the origins of the Hund multiplicity rule for two-dimensional, two-electron quantum dots by visualizing the internal part of the wave function. This in turn was made possible thanks to the special characteristics of our model: the two-electron nature admits the separation of the orbital and spin degrees of freedom, the harmonic nature of the confining potential allows the separation of the center-of-mass and of the internal degrees of freedom, and a low dimensionality of our model (less than 3) reduces the dimension of the internal space to as small as two, allowing a direct visualization of the internal wave functions within the xy plane. Indeed, this has been precisely the reason for our choice of this model. Although our results pertain, strictly speaking, to artificial atoms, they undoubtedly enhance our understanding of Hund's multiplicity rule in general, particularly thanks to the fact that our model enables a smooth transition from the regime in which the conventional interpretation operates [17] to the regime characterizing the actual atomic or molecular systems [18–23] depending on the strength of the confinement ω_{xy}.

[1] N. F. Johnson, J. Phys.: Condens. Matter **7**, 965 (1995).

[2] S. Tarucha, D. G. Austing, T. Honda, R. J. van der Hage, and L. P. Kouwenhoven, Phys. Rev. Lett. **77**, 3613 (1996).

[3] R. C. Ashoori, Nature (London) **379**, 413 (1996).

[4] L. Kouwenhoven, T. H. Oosterkamp, M. W. S. Danoesastro, M. Eto, D. G. Austing, T. Honda, and S. Tarucha, Science **278**, 1788 (1997).

[5] S. Bednarek, B. Szafran, and J. Adamowski, Phys. Rev. B **59**, 13036 (1999).

[6] P. Matagne, J. P. Leburton, D. G. Austing, and S. Tarucha, Physica E **13**, 679 (2002).

[7] F. Hund, *Linienspektren und Periodisches System der Elemente* (Springer, Berlin, 1927), p. 124.

[8] E. U. Condon and G. H. Shortley, *The Theory of Atomic Spectra* (Cambridge University Press, Cambridge, UK, 1935).

[9] G. Herzberg, *Atomic Spectra and Atomic Structure* (Dover, New York, 1944), p. 135.

[10] B. W. Shore and D. H. Menzel, *Principles of Atomic Spectra* (Wiley, New York, 1968), p. 101.

[11] L. Szasz, *The Electronic Structure of Atoms* (Wiley, New York, 1992), p. 52.

[12] H. Friedrich, *Theoretical Atomic Physics* (Springer, Berlin, 2006), p. 105.

[13] F. Hund, *Geschichte der Quantentheorie* (Bibliographisches Institut Wissenschaftsverlag, Zurich, 1975).

[14] M. Schroeder, Ed., *Hundert Jahre Friedrich Hund* (Vanden-Hoeck and Ruprecht, Goettingen, 1996).

[15] A. Sommerfeld, *Atombau und Spektrallinien* (Vieweg, Braunschweig, 1944), 6th ed., Vol. I, p. 486.

[16] G. Herzberg, *Molecular Spectra and Molecular Structure* (Van Nostrand, New York, 1950), 2nd ed., Vol. 1, p. 335.

[17] J. C. Slater, Phys. Rev. **34**, 1293 (1929).

[18] E. R. Davidson, J. Chem. Phys. **41**, 656 (1964).

[19] E. R. Davidson, J. Chem. Phys. **42**, 4199 (1965).

[20] R. J. Boyd and C. A. Coulson, J. Phys. B: Mol. Phys. **6**, 782 (1973).

[21] R. J. Boyd, Nature (London) **310**, 480 (1984).

[22] R. P. Messmer and F. W. Birss, J. Phys. Chem. **73**, 2085 (1969).

[23] J. Katriel, Phys. Rev. A **5**, 1990 (1972).

[24] J. Katriel, Theor. Chim. Acta **23**, 309 (1972).

[25] J. Katriel, Theor. Chim. Acta **26**, 163 (1972).

[26] J. Katriel and R. Pauncz, Adv. Quantum Chem. **10**, 143 (1977).

[27] K. Hongo, R. Maezono, Y. Kawazoe, H. Yasuhara, M. D. Towler, and R. J. Needs, J. Chem. Phys. **121**, 7144 (2004).

[28] G. W. Bryant, Phys. Rev. Lett. **59**, 1140 (1987).

[29] A. P. Alivisatos, Science **271**, 933 (1996).

[30] P. A. Maksym, H. Imamura, G. P. Mallon, and H. Aoki, J. Phys.: Condens. Matter **12**, R299 (2000).

[31] T. Sako and G. H. F. Diercksen, J. Phys.: Condens. Matter **15**, 5487 (2003).

[32] T. Sako and G. H. F. Diercksen, J. Phys.: Condens. Matter **17**, 5159 (2005).

[33] T. Sako and G. H. F. Diercksen, Phys. Rev. B **75**, 115413 (2007).

[34] T. Sako and G. H. F. Diercksen, J. Phys.: Condens. Matter **20**, 155202 (2008).

[35] P. A. Maksym and T. Chakraborty, Phys. Rev. Lett. **65**, 108 (1990).

[36] U. Merkt, J. Huser, and M. Wagner, Phys. Rev. B **43**, 7320 (1991).

[37] C. Yannouleas and U. Landman, Phys. Rev. B **68**, 035325 (2003).

[38] M. B. Tavernier, E. Anisimovas, F. M. Peeters, B. Szafran, J. Adamowski, and S. Bednarek, Phys. Rev. B **68**, 205305 (2003).

[39] Y. Sajeev, M. Sindelka, and N. Moiseyev, J. Chem. Phys. **128**, 061101 (2008).

[40] M. Wagner, U. Merkt, and A. V. Chaplik, Phys. Rev. B **45**, 1951 (1992).

[41] J. T. Lin and T. F. Jiang, Phys. Rev. B **64**, 195323 (2001).

[42] T. Sako and G. H. F. Diercksen, J. Phys. B **36**, 1433 (2003).

[43] T. Sako and G. H. F. Diercksen, J. Phys. B **36**, 1681 (2003).

[44] T. Sako and G. H. F. Diercksen, J. Phys. B **36**, 3743 (2003).

[45] O. Dippel, P. Schmelcher, and L. S. Cederbaum, Phys. Rev. A **49**, 4415 (1994).

[46] W. Becken, P. Schmelcher, and F. K. Diakonos, J. Phys. B **32**, 1557 (1999).

[47] W. Becken and P. Schmelcher, J. Phys. B **33**, 545 (2000).

[48] M. Braskén, M. Lindberg, D. Sundholm, and J. Olsen, Phys. Rev. B **61**, 7652 (2000).

[49] T. Sako, I. Cernusak, and G. H. F. Diercksen, J. Phys. B **37**, 1091 (2004).

[50] T. Sako, S. Yamamoto, and G. H. F. Diercksen, J. Phys. B **37**, 1673 (2004).

[51] S. Corni, M. Braskén, M. Lindberg, J. Olsen, and D. Sundholm, Phys. Rev. B **67**, 085314 (2003).

[52] P. S. Drouvelis, P. Schmelcher, and F. K. Diakonos, J. Phys.: Condens. Matter **16**, 3633 (2004).

[53] P. S. Drouvelis, P. Schmelcher, and F. K. Diakonos, Phys. Rev. B **69**, 035333 (2004).

[54] T. Sako, P. A. Hervieux, and G. H. F. Diercksen, Phys. Rev. B **74**, 045329 (2006).

[55] W. Kohn, Phys. Rev. **123**, 1242 (1961).

[56] L. Brey, N. F. Johnson, and B. I. Halperin, Phys. Rev. B **40**, 10647 (1989).

[57] F. M. Peeters, Phys. Rev. B **42**, 1486 (1990).

[58] Q. P. Li, K. Karräi, S. K. Yip, S. Das Sarma, and H. D. Drew, Phys. Rev. B **43**, 5151 (1991).

[59] J. F. Dobson, Phys. Rev. Lett. **73**, 2244 (1994).

[60] M. Pi, F. Ancilotto, E. Lipparini, and R. Mayol, Physica E **24**, 297 (2004).

[61] T. Sako, J. Paldus, and G. H. F. Diercksen, Adv. Quantum Chem. **58**, 177 (2009).

[62] M. Taut, J. Phys. A: Math. Gen. **27**, 1045 (1994).

[63] M. Taut, Phys. Rev. A **48**, 3561 (1993).